



Cite this: *J. Mater. Chem. C*, 2017, 5, 5718

# Dynamic nature of excited states of donor–acceptor TADF materials for OLEDs: how theory can reveal structure–property relationships†

Yoann Olivier,<sup>\*a</sup> Mónica Moral,<sup>b</sup> Luca Muccioli<sup>cd</sup> and Juan-Carlos Sancho-García<sup>e</sup>

Spin statistics greatly limits the efficiency of OLEDs, which might be largely improved upon conversion of triplet into singlet-excited (and thus light-emitting) states via a Thermally Activated Delayed Fluorescence (TADF) process. We theoretically investigate here the combination of some real-life donor (D) and acceptor (A) moieties with the connectivity D–A and D–A–D. We selected phenoxazine (PXZ) and phenylthiazine (PTZ) as electron-donating groups, and 2,5-diphenyl-1,3,4-oxadiazole (OXD), 3,4,5-triphenyl-4*H*-1,2,4-triazole (TAZ), and 2,5-diphenyl-1,3,4-thiadiazole (TDZ) as their electron-accepting partners. The systematic Tamm–Dancoff Approximation-Density Functional Theory calculations performed allowed us to calculate accurately not only the energy levels of low-lying singlet and triplet-excited states, but also to characterize their Charge-Transfer (CT) or Locally Excited (LE) nature, since the energy difference and the coupling between the <sup>3</sup>CT, <sup>3</sup>LE, and <sup>1</sup>CT states become key to understanding the molecular mechanism involved in this process. We have also studied the role played by the conformational landscape, arising from the thermally accessible range of D–A(–D) torsion angles, in the singlet–triplet energy gap as well as its influence on oscillator strengths. Overall, we rationalize the origin of the higher efficiencies found in real devices for D–A–D molecules, disclosing the underlying structure–property relationships and thus anticipating successful design strategies.

Received 22nd November 2016,  
Accepted 20th December 2016

DOI: 10.1039/c6tc05075a

www.rsc.org/MaterialsC

## 1 Introduction

The development of Organic Light-Emitting Diodes (OLEDs) has experienced a constant and rapid improvement over recent

years, leading to the first commercial applications. For the process of producing OLEDs for lighting, or multicolor displays, materials capable of emitting in the red, green and blue regions of the visible spectrum have to be synthesized and the corresponding device efficiently manufactured.<sup>1–4</sup> State-of-the-art OLEDs have a multi-layer architecture where the most important role is played by hole/electron injecting layers, to ease charge injection, and hole/electron blocking layers, to confine the charge carriers to the Emission Layer (EML). When focusing on the EML, the main factor inhibiting the Internal Quantum Efficiency (IQE) is the unfavorable spin statistics when charges combine to form excitons.<sup>5,6</sup> Indeed, only 25% of light emitting singlet excited-states ( $S_1$ ) versus the 75% of non-emissive triplet excited-states ( $T_1$ ) are created, limiting the external quantum efficiency (EQE) of fluorescent emitters to 5% when considering an out-coupling efficiency of 20%. So far, one of the most employed strategies in order to maximize the IQE of these devices relies on the use of compounds containing heavy metals such as Iridium or Platinum with a large spin–orbit coupling, making phosphorescence activity (emission from the in principle dark  $T_1$  state) reliable enough, thus avoiding energy losses through non-radiative processes.<sup>7</sup>

As an alternative to the use of costly and/or possibly toxic phosphorescent metal complexes, new fully organic materials relying on the Thermally Activated Delayed Fluorescence (TADF)

<sup>a</sup> Laboratory for Chemistry of Novel Materials, University of Mons, 7000 Mons, Belgium. E-mail: yoann.olivier@umons.ac.be

<sup>b</sup> Renewable Energy Research Institute University of Castilla-La Mancha, 02071 Albacete, Spain

<sup>c</sup> Institut des Sciences Moléculaires, UMR 5255, University of Bordeaux, 33405 Talence, France

<sup>d</sup> Dipartimento di Chimica Industriale “Toso Montanari”, University of Bologna, 40136 Bologna, Italy

<sup>e</sup> Departamento de Química Física, University of Alicante, 03080 Alicante, Spain

† Electronic supplementary information (ESI) available: (i) Isocontour plots of the calculated frontier orbitals (HOMO and LUMO), (ii) excited states diagrams of all the monomers (PXZ, OXZ, TAZ, PTZ, TDZ) and the corresponding D–A and D–A–D combinations studied, (iii) plots of the oscillator strengths normalized to the  $S_1$  transition energy as a function of  $[\phi_S(S_1)]^2$  and (iv) torsion energy profiles,  $\Delta E^{ST}$ ,  $\phi_S(S_1)$  and  $\phi_S(T_1)$  as a function of the torsion angles between the acceptor units (OXD, TDZ and TAZ) with the two PXZ donors for 2PXZ–OXD, 2PXZ–TDZ and 2PXZ–TAZ, tables reporting (iv) the relative energies between the axial and the equatorial conformers, (v) tables with  $S_1$ ,  $T_1$  energies and their associated  $\phi_S$  and  $\Delta r$  values as well as the oscillator strengths for both axial and equatorial conformers, (vi) equilibrium D–A torsion angle for the optimized ground-state,  $S_1$  and  $T_1$  geometries and (vii) NTO representation of the excited states of equatorial compounds. See DOI: 10.1039/c6tc05075a

mechanism have been recently developed<sup>8–11</sup> to ease the conversion of the non-emissive triplet excitons to emissive singlet states by a (Reverse) InterSystem Crossing ((R)ISC) mechanism. In TADF materials, the usual prompt fluorescence occurring on the sub-nanosecond timescale is followed by a long-lived component typically on the micro- to the millisecond scale, the so-called delayed fluorescence resulting from the interconversion of triplet excitons into singlets. Knowing that phosphorescent compounds are able to achieve an External Quantum Efficiency (EQE) close to 30%,<sup>12,13</sup> competitive values around 30% have been already obtained<sup>5</sup> for devices made of purely organic host matrices and TADF green emitters, while blue emitters are still lagging behind with an EQE of around 20%<sup>14</sup> leaving thus room for further improvement.

The general strategy to maximize the conversion of triplets into singlets consists in minimizing the spatial overlap between the HOMO (Highest Occupied Molecular Orbital) and LUMO (Lowest Unoccupied Molecular Orbital) frontier orbitals in order to minimize the exchange energy and bring the singlet and triplet excited states close together. This is usually achieved in donor–acceptor (D–A) compounds where the HOMO (LUMO) is primarily localized on the donor (acceptor) moiety. As a consequence of this large spatial separation, the lowest singlet and triplet excitations usually feature a strong intramolecular charge-transfer (ICT) character, which is not always compatible with intense emission requirements (high oscillator strength and large transition dipole moment).<sup>15</sup> The choice of the donor and the acceptor appears to be very crucial since in some instances, a Locally Excited triplet state (<sup>3</sup>LE) localized either on the donor or the acceptor becomes more stable than the charge transfer (CT) states, thus hindering the triplet to singlet interconversion and leading to inefficient TADF.<sup>16</sup> To date, the main picture that has arisen to explain the TADF mechanism involves the interconversion between the <sup>3</sup>CT and <sup>1</sup>CT states.<sup>2–6</sup> However, more recently, Monkman and co. hypothesized a key role of the presence of a <sup>3</sup>LE state in near resonance with the CT states, which might lead to an enhancement of the interconversion mechanism. This appears to be a consequence of a larger <sup>3</sup>LE–<sup>1</sup>CT spin–orbit coupling in comparison to the <sup>3</sup>CT–<sup>1</sup>CT one, because of the different spatial localization of the involved states.<sup>17–19</sup> As an alternative to these mechanisms driven by spin–orbit coupling, interconversion driven by hyperfine couplings has also been reported but appears to be a negligible pathway since its contribution requires an energy spacing between the <sup>3</sup>CT and <sup>1</sup>CT states below 1 cm<sup>–1</sup>.<sup>20</sup> Even though the detailed mechanism of TADF is still under debate, the interconversion between triplet and singlet excitons clearly involves excited states carrying a significant CT character.

On the computational side, identifying and benchmarking a protocol capable of accurately estimating the difference in energy between the singlet and triplet states, as well as of classifying their nature (either LE or CT) for designing promising materials, remains a challenging task because of the lack of a well-established methodology capable of simultaneously describing (singlet and triplet) CT states. Since the presence of ICT states seems to be co-substantial with the nature itself of

an efficient interconversion mechanism, the blind application of density functional theory (DFT) remains a challenge, and thus fine-tuned exchange–correlation functionals are used, that is, employing a different weight of exact-like exchange<sup>21</sup> or optimizing the range-separation parameter<sup>22,23</sup> for each compound, making this procedure not transferable to new candidates.<sup>21</sup> With a somewhat different goal, recent studies pursued the computational screening of any possible host/guest system from a set of defined fragments without any experimental information, through the use of machine-learning approaches capable of identifying the potential of candidate emitters when used in devices.<sup>24,25</sup> Even though this approach might be highly useful for initial studies of unknown molecules, or for preliminary or blind screening, it still suffers from reported uncertainties of around ±0.3 eV in the evaluation of  $\Delta E^{\text{ST}}$ , the energy gap between the singlet and triplet lowest excited states and calls for more accurate estimates to disclose any molecular design rules.

So far, the most common strategy for designing new TADF emitters relies on the donor–acceptor (D–A) approach.<sup>26</sup> The amount of electronic interaction between these moieties needs to be well-balanced in order to obtain the singlet and triplet CT (as well as the <sup>3</sup>LE) states close in energy and HOMO (LUMO) orbital mainly localized on the donor (acceptor) unit. The D–A electronic interaction can be tuned by engineering (i) the energy offset between the frontiers orbitals, (ii) the molecular symmetry, (iii) the geometrical and sterical constraints (*i.e.* dihedral angle between the D and the A) and (iv) by using a connector between them. However the final outcome is always a compromise between the contrasting requirements of spacial separation of the orbitals (to minimize  $\Delta E^{\text{ST}}$ ) and a non-negligible overlap (to gain sufficient oscillator strength and make light emission possible).

Besides D–A materials, where a single D is grafted to the A unit, recent literature demonstrates the rise of compounds where several donors are attached to the acceptor unit, achieving low  $\Delta E^{\text{ST}}$  and presenting particularly high EQEs.<sup>5,14,27–29</sup> Adachi and co. have synthesized symmetric D–A–D compounds containing phenoxazine (PXZ) as an electron donor, and 2,5-diphenyl-1,3,4-oxadiazole (OXD) as an electron acceptor, **2PXZ–OXD**, or 3,4,5-triphenyl-4H-1,2,4-triazole (TAZ) as an acceptor, **2PXZ–TAZ**. These D–A–D have shown PhotoLuminescence Quantum Yields (PLQYs) larger than their D–A parent compounds (*i.e.* **PXZ–OXD** and **PXZ–TAZ**) in toluene solution.<sup>30</sup> In addition, **2PXZ–TAZ** and **PXZ–TAZ** are quite remarkable, since they display sky blue-emission, a feature of particular interest considering the relatively few available blue TADF emitters.<sup>14</sup> With a similar molecular design approach, the same authors have also introduced 2,5-diphenyl-1,3,4-thiadiazole (TDZ) to replace OXD, leading to a reduced  $\Delta E^{\text{ST}}$ , a shift to the orange of the emission maximum and an increased contribution of the delayed component of the fluorescence to the EQE, attributed to a reduced  $\Delta E^{\text{ST}}$  in comparison to **2PXZ–OXD**.<sup>31</sup>

Since we recently benchmarked a methodology<sup>32</sup> capable of providing deviations as low as 0.1 eV for the  $\Delta E^{\text{ST}}$  energy gap with respect to the experimental results, in this study, we aim at applying it to the characterization of the excited states

properties of (2)PXZ–OXD and (2)PXZ–TAZ compounds. Owing to the relatively simple structure of the D–A(–D) compounds, we have systematically changed the nature of the electron-donating and accepting groups to study their impact on the magnitude of  $\Delta E^{ST}$ . We consider in addition to PXZ, phenothiazine (PTZ) as a second donor. Analogous to PXZ, PTZ is a convenient electron donor in various applications such as dye-sensitized solar cells,<sup>33,34</sup> polymer field-effect transistors<sup>35</sup> and light-emitting diodes.<sup>36–38</sup> Similarly, we have increased the strength of the acceptor group by investigating TAZ, OXD and TDZ, respectively. The combination of the different electron donors and acceptors results in six D–A and six D–A–D molecules (see Fig. 1), whose excited and ground states are thoroughly characterized in the following. In addition, since it was

previously<sup>39</sup> shown when considering PTZ as an electron donor and a triphenyl-triazine electron acceptor (TRZ) that PTZ–TRZ exists in two distinct conformations, namely the (quasi)-axial (almost coplanar D and A units) and the (quasi)-equatorial (large torsion angle between the D and A units) conformations, we consider and compare both conformers for all compounds.

## 2 Computational details

We optimize in all cases the ground-state ( $S_0$ ) geometry of the compounds with the PBE0-D3(BJ) method,<sup>40,41</sup> including the -D3(BJ) correction for intra-molecular (if any) dispersion effects.<sup>42–44</sup> We then compute the vertical excitation energies

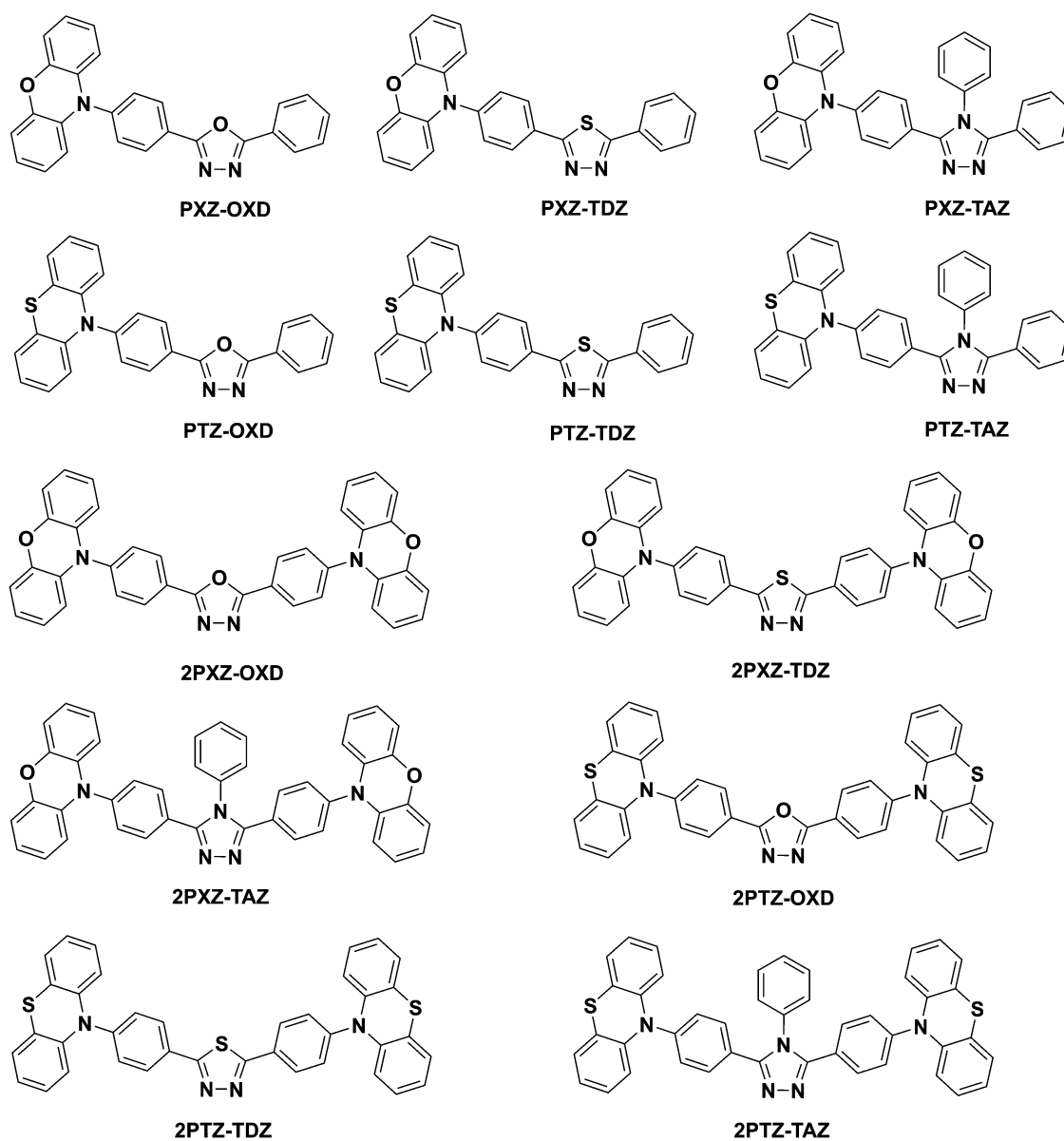


Fig. 1 Chemical structures and shortened names of the investigated compounds. The hydrogen atoms and corresponding C–H bonds have been omitted for clarity.

for absorption to the  $S_1$  ( $E_V(S_1)$ ) and  $T_1$  ( $E_V(T_1)$ ) excited-states, which gives correspondingly the vertical singlet–triplet gap as  $\Delta E_{V}^{ST} = E_V(S_1) - E_V(T_1)$ . We also calculate the adiabatic  $\Delta E_A^{ST} = E(S_1) - E(T_1) = \Delta E_V^{ST} - \lambda_{S_1} + \lambda_{T_1}$  where  $\lambda_{S_1}$  and  $\lambda_{T_1}$  are the relaxation energies calculated in the  $S_1$  and  $T_1$  states and which are calculated as  $\lambda_{S_1} = E_V(S_1) - E(S_1)$  and  $\lambda_{T_1} = E_V(T_1) - E(T_1)$  where  $E(S_1)$  and  $E(T_1)$  represent the energy of the optimized  $S_1$  and  $T_1$  states, respectively. All excited state energies (relaxed and unrelaxed) are calculated within the Tamm–Dancoff approximation (TDA)<sup>45</sup> to the linear-response time-dependent (TD)-DFT approach, which significantly and systematically improves the accuracy of triplet energies<sup>46–48</sup> and  $\Delta E^{ST}$  values. We consequently include the solvent effects by the non-equilibrium Polarizable Continuum Model (PCM) using the integral equation formalism variant (IEF-PCM) for hybrid (*i.e.* PBE0) methods both for the geometry optimization and excited state calculations.<sup>49,50</sup> All calculations have been performed with the GAUSSIAN09 D.01 package.<sup>51</sup> In order to choose the basis set, we have compared in Tables S1 and S2 (ESI<sup>†</sup>) the 6-31G(d,p) and def2-TZVP<sup>52</sup> ones and verified that they lead to similar relative energies between the axial and the equatorial conformers. Interestingly, all equatorial (2)PXZ derivatives are sensibly more stable than the axial ones, while both axial and equatorial (2)PTZ conformers are almost isoenergetic and will most likely coexist.

In Tables S3 and S4 (ESI<sup>†</sup>) for the equatorial conformer and in Table 2 and Table S5 (ESI<sup>†</sup>) for the axial conformer, we have further compared  $\Delta E_{V}^{ST}$  calculated with the 6-31G(d,p) and the def2-TZVP basis sets and we have found small differences between the two. On the basis of these results, we adopted the smallest 6-31G(d,p) basis set that considerably reduces the computational time when computing the excited state properties, and, in particular, when searching for the energy minimum on the singlet and triplet excited state potential energy surfaces.

Furthermore, we perform some post-processing of the results in order to determine quantitatively, the nature of the calculated excited states. Previously, we have stressed the importance of referring to Natural Transition Orbitals (NTOs) when analyzing the reorganization of the electronic density upon electronic transition to the excited states.<sup>32</sup> To characterize the spatial separation of the frontier orbitals, we have introduced a metric based on the hole and electron distance  $\Delta r$ , inversely proportional to the experimentally measured and/or calculated  $\Delta E^{ST}$  values. In a recent attempt to classify compounds for OLED applications, Chen *et al.*<sup>53</sup> have established, in addition to  $\Delta r$ , a metric  $I$  based on the absolute value of the Highest Occupied NTO (HONTO) and the Lowest Unoccupied NTO (LUNTO) overlap, similar to the  $A$  metric developed by Tozer and co.<sup>47,54</sup> They found that compounds with small  $I$  for both  $S_1$  ( $I_S$ ) and  $T_1$  ( $I_T$ ) and large  $\Delta r_S$  and  $\Delta r_T$ , compatible with  $S_1$  and  $T_1$  bearing a large CT character, are conditions to minimize their  $\Delta E^{ST}$  values. Here, we rely on the more compact attachment/detachment formalism.<sup>55,56</sup> Indeed, in this approach, the difference density matrix between the ground and an excited state is diagonalized to obtain the occupation numbers (eigenvectors) and orbitals (eigenvalues) for each electronic transition selected. The detachment

(attachment) density matrix is obtained by summing up over the eigenvectors possessing negative (positive) occupations, weighted by the absolute value of their occupations. Instead of referring to the HONTO and LUNTO orbitals, in the attachment/detachment approach it is possible to directly access the localization of the electron density of the ground state that is removed upon electronic excitation (*i.e.* the detachment density matrix) and rearranged in the excited state (*i.e.* the attachment density) by considering all the orbitals characteristic of the electronic transitions. The attachment and detachment densities are often seen as the hole and electron densities, respectively. From these results, we have computed two metrics to identify and quantify CT excited-states, namely the averaged  $\Delta r$ <sup>57</sup> and  $\phi_S$ <sup>58,59</sup> the overlap between the attachment and detachment density matrices. Both metrics are computed using the NANCY\_EX package<sup>58,59</sup> and allow us to unambiguously determine the nature of the excited states being either ICT or LE.

## 3 Results and discussion

### 3.1 Equatorial conformers

**3.1.1 Frontier orbitals characterization.** We first start by investigating the shape and energy of the frontier orbitals of the different D–A and D–A–D equatorial conformers (*i.e.* with a D–A dihedral angle of about 90 degrees) and of their constituting D and A units (see Fig. 2 and Fig. S1–S5, ESI<sup>†</sup>). Among the two donors initially investigated, PXZ appears to have a slightly stronger donor character than PTZ as well as a larger band gap. We also observe that TDZ has the strongest acceptor character, followed by OXD and TAZ. The almost perpendicular arrangement of D and A aromatic planes with respect to each other (see Table S6, ESI<sup>†</sup>) guarantees a good spatial separation of the respective frontier orbitals at the expense of a weak orbital overlap. We note that the HOMO and (H–1)OMO levels of D–A–D compounds are (nearly) degenerated due to the high symmetry that is retained throughout the optimization of the geometries (see Table 1 for the symmetry point groups at the optimized equatorial geometry). The HOMO and (H–1)OMO orbital shapes are quite similar being the anti-bonding and the bonding linear combination of the HOMO of PXZ or PTZ. When comparing their HOMO energies, we observe almost no change in energy (in agreement with the experiment,<sup>31</sup> see Fig. S6, ESI<sup>†</sup>) and orbital shapes when comparing PXZ or PTZ and their corresponding D–A and D–A–D compounds, highlighting the weak electronic interaction between the HOMOs of D and A. Conversely, despite exhibiting similar or larger LUMO energy separation, the D–A and D–A–D LUMOs appear to be around 0.2 and 0.4 eV stabilized with respect to the LUMO level of the acceptors, emphasizing higher electronic interaction between the LUMOs of the D and the A units. Therefore, a decrease in the energy band gap is observed when going from D–A to D–A–D molecules. Based on these frontier orbitals diagrams (see Fig. 2 and Fig. S1–S5, ESI<sup>†</sup>), in a first approximation the bluest compounds are obtained for D–A with TAZ acceptor, due to the higher-lying LUMO orbital of this unit.

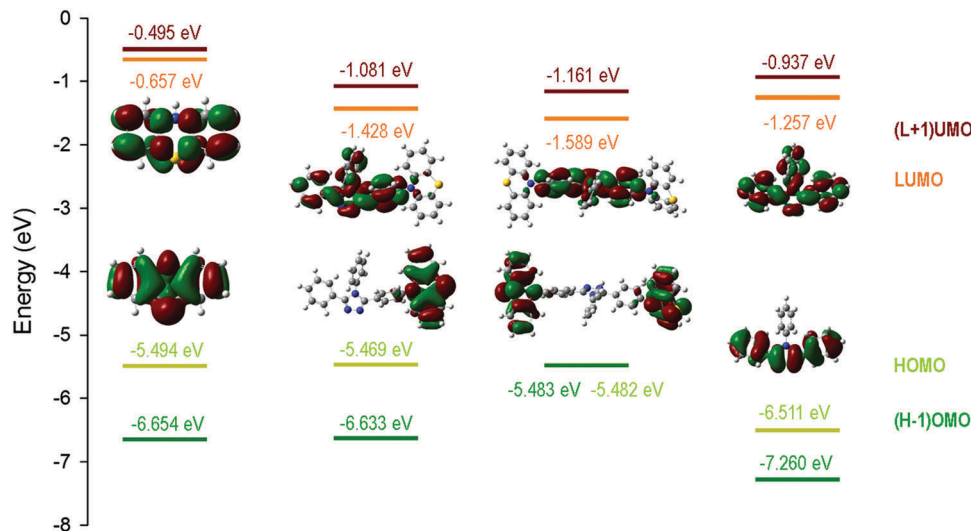


Fig. 2 Isocontour plots (cutoff = 0.02 a.u.) and energy of the frontier orbitals (HOMO and LUMO) calculated at the PBE0-D3(BJ)/6-31G(d,p) level of theory with the PCM module for solvent (toluene), for the case of combining PTZ (right) with TAZ (left) moieties giving rise to the **PTZ-TAZ** and **2PTZ-TAZ** equatorial conformers (center). The size and color describe the amplitude and sign, respectively, of the lobes of orbitals.

Table 1 Calculated excited states energy values ( $E$ ), oscillator strengths (O.S.<sup>a</sup>),  $\phi_s$ ,  $\Delta r$  as well as the dominant character of these transitions for the equatorial **2PXZ-OXD** and **2PTZ-TAZ** conformers. In bold, the corresponding  $S_1-T_1$  energy difference

State	<b>PXZ-OXD</b> ( $C_s$ )				<b>PTZ-TAZ</b> ( $C_1$ )					
	$E$ (eV)	O.S.	$\phi_s$	$\Delta r$ (Å)	CT/LE	$E$ (eV)	O.S.	$\phi_s$	$\Delta r$ (Å)	CT/LE
$T_1$	2.593	—	0.15	5.58	CT	3.177	—	0.72	0.85	LE
$S_1$	2.604	0	0.15	5.62	CT	3.345	$4 \times 10^{-4}$	0.23	4.98	CT
$T_2$	3.037	—	0.79	0.12	LE	3.371	—	0.44	4.26	CT
$\Delta E^{ST}$	<b>0.011</b>					<b>0.168</b>				

State	<b>2PXZ-OXD</b> ( $C_s$ )				<b>2PTZ-TAZ</b> ( $C_2$ )					
	$E$ (eV)	O.S.	$\phi_s$	$\Delta r$ (Å)	CT/LE	$E$ (eV)	O.S.	$\phi_s$	$\Delta r$ (Å)	CT/LE
$T_1$	2.478	—	0.16	1.85	CT	3.165	—	0.64	0.46	CT-LE
$T_2$	2.478	—	0.16	1.85	CT	3.165	—	0.64	0.46	CT-LE
$S_1$	2.939	0	0.17	5.75	CT	3.266	0	0.22	0.93	CT
$S_2$	2.488	0	0.15	1.86	CT	3.267	$3 \times 10^{-4}$	0.22	0.93	CT
$T_3$	3.021	—	0.78	0.01	LE	3.311	—	0.51	0.67	CT-LE
$T_4$	3.021	—	0.78	0.01	LE	3.312	—	0.51	0.67	CT-LE
$\Delta E^{ST}$	<b>0.010</b>					<b>0.101</b>				

<sup>a</sup> Note that the oscillator strengths are only defined for singlet excitations.

**3.1.2 Excited states calculations and characterization.** Not surprisingly, the TDA calculations confirm that the  $S_1$  and  $T_1$  states of D-A-D molecules are red-shifted with respect to the D-A ones and that the bluest compounds are obtained when a TAZ acceptor is considered (see Table S3, ESI<sup>†</sup>). We also mention that correct color ordering, *i.e.*, theoretically determined relative energies for absorption agree with the ordering experimentally found for the compounds actually synthesized (**2PXZ-OXD**, **2PXZ-TAZ** and **2PXZ-TAZ**).<sup>30,31</sup> Among the proposed new molecules, **2PTZ-TAZ** appears to be even bluer than the sky-blue **2PXZ-TAZ** compound ( $S_1$  is roughly 0.3 eV higher in energy, see Table S3, ESI<sup>†</sup>). In great contrast with the

experiments, the whole set of compounds exhibit vanishing oscillator strengths (O.S.) for their lowest singlet excited states. Previous theoretical estimates<sup>30</sup> at the CAM-B3LYP/cc-pVDZ level reported similar negligible values for all cases studied (**PXZ-OXD**, **PXZ-TAZ**, **2PXZ-OXD**, and **2PXZ-TAZ**). We are also aware that the TDA causes the oscillator strengths to incur in some error,<sup>60</sup> since the  $f$ -sum rule, also known as the Thomas-Reiche-Kuhn sum rule, is no longer fulfilled exactly. However, we have carefully checked this point by rerunning some calculations at the full TD-DFT level, without noticing significant changes in the O.S. values. We have also carefully observed that the low oscillator strengths of  $S_1$  excitations are not due to symmetry-forbidden transitions but are a consequence of the large twist angle between D and A units, which offers a poor overlap between the frontier orbitals. Moreover, the magnitude of the oscillator strengths of the  $S_1$  transitions does not increase even when considering geometry relaxation towards the energy minimum of  $S_1$  potential energy surface. Indeed, in the excited state, we note a further increase of D-A torsion angles (even closer to 90 degrees, see Table S6, ESI<sup>†</sup>) irrespective of the donor and the acceptor, which is characteristic of a Twisted Intramolecular Charge Transfer (TICT) state.<sup>61</sup>

In their classification, Chen *et al.*<sup>53</sup> distinguished three types of materials depending on the extent of the separation  $\Delta r$  between the HONTO and LUNTO centroids as well as the overlap  $I$  between these two NTOs for both  $S_1$  and  $T_1$ . For efficient TADF materials, both  $\Delta r_S$  and  $\Delta r_T$  must be large, as well as  $I_S$  and  $I_T$  must be small. Here, we characterize the excited properties of the different molecules using  $\Delta r$  calculated in terms of the attachment/detachment formalism, with  $\phi_s$  the overlap between the corresponding densities. Typically, a  $\Delta r$  larger than 1.5–2.0 Å has been proposed before to identify a CT excitation,<sup>57</sup> while  $\phi_s$  amounts to 0 (1) when the electronic transition bears an charge-transfer character (is [LE]) by nature. Intermediate values

describe excitations exhibiting a mixed CT-LE character with either dominant CT or LE character depending on if  $\phi_s$  is smaller or larger than 0.5, respectively.

All the D-A molecules display a similar electronic structure with  $T_2$  lying above  $T_1$  and  $S_1$  while for the D-A-D ones,  $S_1$  and  $S_2$  lie above  $T_1$  and  $T_2$  and below  $T_3$  and  $T_4$ . The presence of two singlet states close in energy certainly explains the broader absorption profiles observed experimentally for D-A-D compounds with respect to D-A molecules.<sup>29</sup> Indeed, each bright state can come up with its own absorption broadening, summing up, which results in a wider absorption band. To characterize the nature of these states, in Table 1 we have reported for **PXZ-OXD** and **PTZ-TAZ** the  $\Delta r$  values corresponding to  $S_1$  and observed that they are largely above the commonly adopted threshold to characterize CT-like transition, with values ranging from 4.0 to 6.5 Å. In addition, the  $\phi_s$  values for these states are all below 0.5 which allows us to establish that the electronic transitions to  $S_1$  have a dominant CT character. **PXZ-OXD**, which is representative of all D-A compounds studied here with the exception of **PTZ-TAZ**, exhibits a  $T_1$  ( $T_2$ ) state with a marked as CT-like (LE) character with  $\Delta r$  largely above 2.0 Å (close to 0 Å) and  $\phi_s$  close to 0 (1). In a NTO analysis,  $S_1$ ,  $T_1$  and  $T_2$  excitations appear to be also in this case dominated by HONTO to LUNTO excitations (see Table S7, ESI†).

We further confirm the nature of these transitions (CT-like for  $S_1$  and  $T_1$  and LE-like for  $T_2$ ) by inspecting their respective attachment/detachment electronic densities (see Fig. 3 left panel for example, for **PXZ-OXD**). Typically, CT (LE) transitions involve a large (small) electronic reorganization of the density from the donor to acceptor unit. As suggested by  $\Delta r$  and  $\phi_s$  values, the triplet states of **PTZ-TAZ** exhibit an opposite nature with respect to **PXZ-OXD**, namely  $S_0$ - $T_1$  and  $S_0$ - $T_2$  transitions are LE- and CT-like, respectively, while  $S_0$ - $S_1$  keeps its CT-character (see Fig. 3 right panel). The hole and the electron densities of  $S_0$ - $T_1$  excitation are mainly localized on the PTZ units, similarly to type I compounds described by Milián-Medina and Gierschner<sup>26</sup> for which the electronic interaction between D and A units is extremely weak.

A qualitative estimate of the singlet (triplet) D-A electronic couplings is given in a state representation by the energy splitting between the  $S_1$  ( $T_1$ ) states of D and A units, assuming that the resulting  $S_1$  ( $T_1$ ) state of the D-A molecule is mainly determined by a bonding combination of the  $S_1$  ( $T_1$ ) states of D and A moieties. Here, one can guess the evolution of the electronic coupling by considering the energy stabilization of the  $S_1$  ( $T_1$ ) state with respect to the  $S_1$  ( $T_1$ ) states of the D and A units. In Fig. 4 and Fig. S7-S10 (ESI†), we have used such a representation for the lowest singlet and triplet excited states of the individual D and A units, as well as for the combinations D-A and D-A-D. The stabilization in energy of the  $T_1$  states of D-A compounds is the lowest for **PTZ-TAZ**, confirming that the electronic interaction between the  $T_1$  states of the D and A units is the weakest for this compound among all. The choice of the donor moiety is crucial since the PTZ donor tends to reduce D-A electronic interactions, an effect which is attributed to a bigger deviation from planarity for PTZ with respect to PXZ (see Fig. S11, ESI†). The non-planarity of the TAZ acceptor (see Fig. S12, ESI†) further contributes to reduced D-A electronic interactions, in line with the lowest triplet stabilization energy and the largest  $\phi_s(T_1)$  values observed for **PXZ-TAZ** and **PTZ-TAZ** (see Table S3, ESI†). Hence, depending on the respective conformation of the donor and the acceptor, it is possible to induce at will either a LE or a CT character to  $T_1$ . We note that the stabilization of  $S_1$  states in the D-A structure with respect to the isolated PTZ and TAZ is not affected by the lack of planarity. Indeed, in contrast with singlet excited states, triplets are subject to the exchange energy which increases their spatial confinement and enhances their LE character.<sup>62,63</sup>

Concerning D-A-D compounds, all of them, with the exception of **2PXZ-OXD** and **2PTZ-OXD**, have  $\Delta r$  values close to 0 Å for all excited states transitions (see Table 1 and Table S3, ESI†) as expected for symmetric molecules.<sup>59</sup> This is not necessarily an indication of LE character, but a mathematical limitation of the  $\Delta r$  metrics, that may hide the true nature of the excited states of D-A-D highly symmetric compounds.<sup>59</sup> For **2PXZ-OXD** and **2PTZ-OXD**,  $\Delta r$  for  $T_1$ ,  $T_2$ ,  $S_1$  and  $S_2$  ranges between 1.7 and 1.8 Å

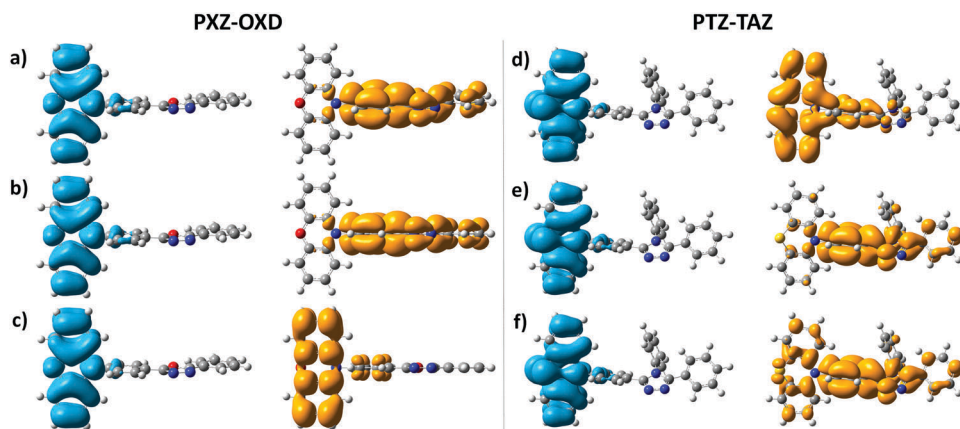


Fig. 3 Hole (blue isocontour) and electron (orange isocontour) densities (cutoff = 0.02 a.u.) obtained in the attachment/detachment formalism from TDA-PBE0-D3(BJ)/6-31G(d,p) calculations with the PCM module for solvent (toluene), for (left panel) **PXZ-OXD** and (right panel) **PTZ-TAZ** compounds associated with (a) and (d)  $T_1$ , (b) and (e)  $S_1$  and, (c) and (f)  $T_2$  excited states.

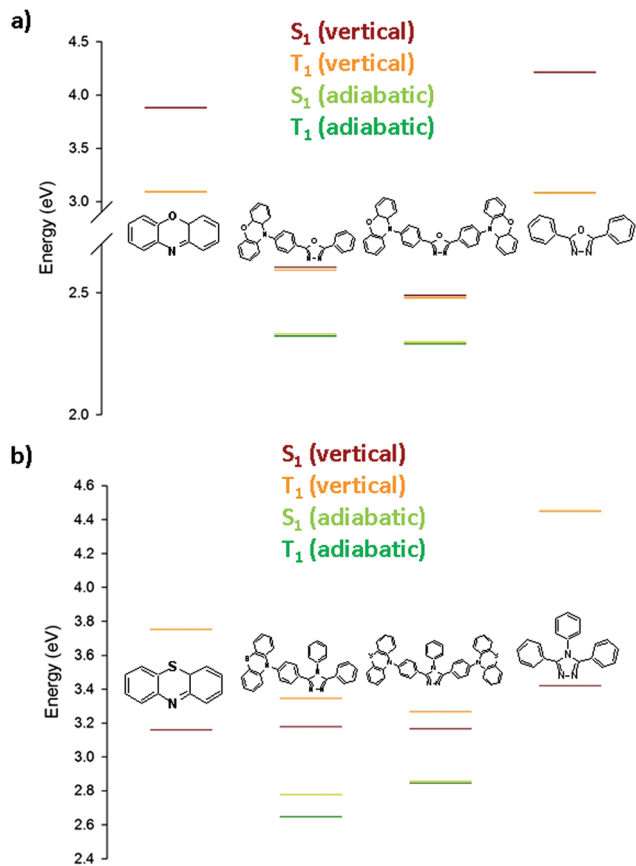


Fig. 4 Excited states energy diagram for the case of combining PXZ (right) with OXD (left) moieties giving rise to the **PXZ–OXD** and **2PXZ–OXD** equatorial conformers (center), as obtained from TDA-PBE0-D3(BJ)/631G(d,p) calculations with the PCM module for solvent (toluene).

because of the V-shape of the OXD acceptor (see Fig. S13, ESI†) which points to a dependence of  $\Delta r$  on detailed geometrical aspects. Similar to D–A compounds, the lowest triplet states of D–A–D molecules bear a strong CT character, with the exception of **2PTZ–TAZ** for which a weaker CT character is observed (see Table 1 and Table S3). Grafting an additional donor to **PTZ–TAZ** does not further stabilize the  $T_1$  state, however, allows for the electron density to further delocalize on the acceptor unit (see Fig. 5 right panel) compared to its corresponding D–A compound

(see Fig. 3 right panel). This rises the CT character of  $T_1$ , confirmed by the decrease of  $\phi_S(T_1)$  compared to **PTZ–TAZ**. In this particular case, the simplified HONTO to LUNTO representation (see Table S7, ESI†) of the different excitations is not appropriate for the description of all excited states and one should invoke the contribution of other pairs of NTOs to complement it. A representation of the different electronic transitions in terms of attachment/detachment electronic densities is therefore more pertinent at increasing complexity of the molecular structure. Finally, analogous to the D–A molecules, the relaxed  $S_1$  states of all studied D–A–D compounds present vanishing oscillator strengths (similarly to  $S_1$  transitions obtained from vertical excitations) due to their TICT character.

**3.1.3 Singlet–triplet gap calculations.** Low values for the vertical  $\Delta E_V^{ST}$  are always obtained, ranging from 0.01 to 0.17 eV for D–A and from 0.01 to 0.1 eV for D–A–D. As expected, going from D–A structures to D–A–D materials results in a slight decrease in  $\Delta E_V^{ST}$  values due to higher stabilization of the  $S_1$  and  $T_1$  states. The largest  $\Delta E_V^{ST}$  are obtained for **PTZ–TAZ** and **2PTZ–TAZ** in line with their largest  $\phi_S(T_1)$  value, *i.e.* their weaker CT character. In this case, the exchange interaction energy is more effective in stabilizing the triplet states and therefore increases the singlet–triplet gap.<sup>62</sup> Still, overall,  $\Delta E_V^{ST}$  is reduced when going from **PTZ–TAZ** to **2PTZ–TAZ** essentially because the  $T_1$  CT character is increased. In such a case, where  $T_1$  holds a LE character, the addition of a second D moiety appears as an interesting design strategy to bring some CT character to  $T_1$  and to subsequently reduce  $\Delta E_V^{ST}$ . We have also evaluated the geometry relaxation of both  $T_1$  and  $S_1$  states for D–A and D–A–D compounds and did not notice major changes in terms of  $\Delta E_A^{ST}$  compared to  $\Delta E_V^{ST}$  for both D–A and D–A–D materials. Interestingly, on one hand, all  $\lambda_{S_1}$  and  $\lambda_{T_1}$  of OXD- and TDZ-based compounds appear to be very similar (see Table 3) most likely to their similar chemical structures and the planar structure of the electron acceptor. On the other hand, TAZ-based compounds exhibit  $\lambda_{S_1}$  and  $\lambda_{T_1}$  that are larger because of the non-planar structure of this electron acceptor. We also see that PXZ-based compounds have overall smaller relaxation energies than PTZ ones, which is consistent with a smaller geometrical reorganization towards a planar conformation of the PXZ unit compared to PTZ. Similarly to reorganization energy in charge transport, the more extended D–A–D compounds

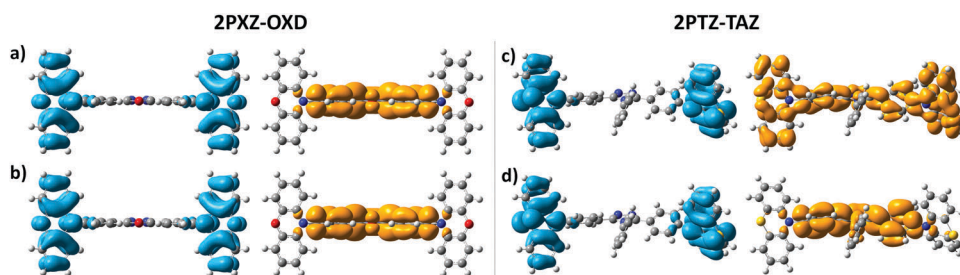


Fig. 5 Hole (blue isocontour) and electron (orange isocontour) densities (cutoff = 0.02 a.u.) obtained in the attachment/detachment formalism from TDA-PBE0-D3(BJ)/6-31G(d,p) calculations with the PCM module for solvent (toluene) for (left panel) **2PXZ–OXD** and (right panel) **2PTZ–TAZ** compounds associated with (a) and (c)  $T_1$ , and, (b) and (d)  $S_1$  excited states.

exhibit smaller  $\lambda_{S_1}$  and  $\lambda_{T_1}$  than D–A ones because of overall smaller variations in molecular degrees of freedom (bonds, angles, dihedral) compared to the ground-state geometry. Finally, the  $\Delta E_A^{ST}$  adiabatic values always remain positive in contrast with the results obtained by Sun *et al.*<sup>23</sup> with PBE and B3LYP functionals.

We compare now our results for the set of molecules (*i.e.* **2PXZ–OXD**, **2PXZ–TDZ** and **2PXZ–TAZ**) for which experimental  $\Delta E^{ST}$  values (obtained from the blue edges of low-temperature fluorescence and phosphorescence spectra) are available.<sup>30,31</sup> Adachi *et al.* measured the singlet–triplet gap of **2PXZ–OXD**,<sup>30</sup> **2PXZ–TDZ**<sup>31</sup> and **2PXZ–TAZ**<sup>30</sup> in doped films (0.15, 0.11 and 0.23 eV, respectively) which compare well with our theoretical estimates (0.01, 0.007 and 0.02 eV for  $\Delta E_V^{ST}$ , see Table S3 (ESI<sup>†</sup>) and 0.008, 0.006 and 0.11 eV for  $\Delta E_A^{ST}$ , see Table 3, respectively) leading to an error of only 0.1–0.2 eV. We will discuss further this discrepancy, just noting here that the previously published values of  $\Delta E_V^{ST}$  calculated at the CAM-B3LYP/cc-pVDZ level<sup>30,31</sup> are affected by a systematic error of 0.4–0.6 eV, in agreement with benchmark studies,<sup>64</sup> which is largely reduced in this work. Indeed, range-separated functionals (*e.g.* CAM-B3LYP) are generally not recommended for triplet states, due to orbital instabilities.<sup>65</sup>

### 3.2 Axial conformers

The evaluation of the torsion potential for the rotation about the D–A bond (see Fig. 6) indicates that for PTZ derivatives, axial conformers are just as stable as the equatorials ones, contrarily to what happens for PXZ derivatives. Of course, axial

derivatives show higher hybridization between the frontier orbitals of donor and the three acceptors resulting in larger delocalization of the HOMO and LUMO orbitals (see for example HOMO and LUMO orbitals in Fig. S14 and S15, ESI<sup>†</sup>) over the whole D–A and D–A–D compounds. Even if some  $\phi_S$  values for  $S_1$  range from 0.64 to 0.95, and are hence compatible with a mixed CT–LE to LE character, the  $\phi_S(T_1)$  values for axial conformers lie in a really narrow range around 0.8, characteristic of a dominant LE character, and accordingly quite large  $\Delta E_V^{ST}$  values (above 0.6 eV) are obtained. In addition, because of the dominant LE character of the lowest singlet and triplet excited states, the  $S_1$  and  $T_1$  energies are significantly blue-shifted compared to the equatorial ones (*cf.* Tables 1, 2 and Table S3, ESI<sup>†</sup>). As a consequence of a large torsional energy barrier (larger than 3 kcal mol<sup>−1</sup> in gas-phase, see Fig. 6), one can expect to observe dual emission from the LE and CT  $S_1$  states of the axial and the equatorial conformers, respectively. Even though the oscillator strengths of the axial conformers are much larger than the equatorial ones, we foresee that most of the fluorescence collected would arise from the equatorial conformer, because, in addition to prompt fluorescence, TADF is expected to take place in equatorial-like conformers in contrast with axial-like conformers.

Furthermore, due to the larger band gap of the axial conformers, efficient Förster energy transfer towards neighboring equatorial conformers could possibly occur. This mechanism was evidenced by Tanaka *et al.*<sup>39</sup> on a PTZ–TRZ TADF emitter. The observed prompt fluorescence of the axial conformer appears to be completely quenched when the temperature increases, which

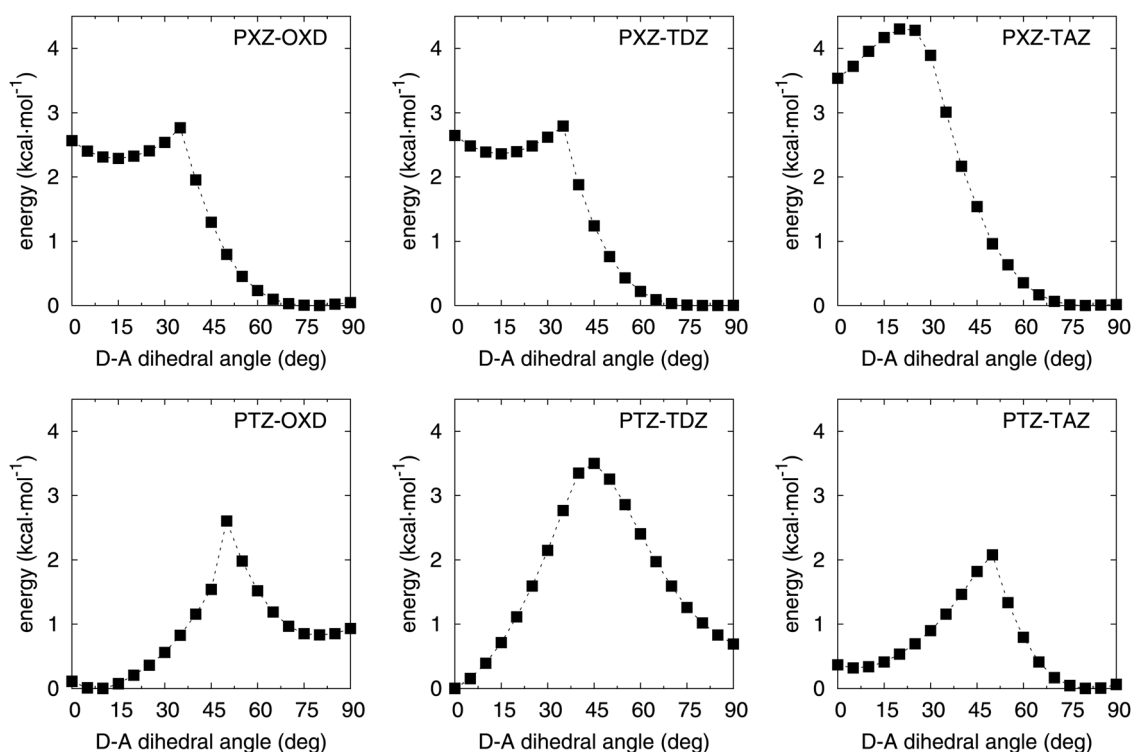


Fig. 6 Torsion profiles calculated at the PBE0-D3(BJ)/6-31G(d,p) level of theory with the PCM module for solvent (toluene) between the different donors (PXZ and PTZ) and acceptors (OXD, TDZ, TAZ).

**Table 2** Calculated excited states energy values ( $E$ ), oscillator strengths (O.S.<sup>a</sup>),  $\phi_s$  and  $\Delta r$  for the whole set of axial conformers. In bold, the corresponding  $S_1$ – $T_1$  energy difference

State	PXZ–OXD			PXZ–TDZ			PXZ–TAZ		
	$E$ (eV)	O.S.	$\phi_s$	$E$ (eV)	O.S.	$\phi_s$	$E$ (eV)	O.S.	$\phi_s$
$T_1$	2.885	—	0.81	2.587	—	0.82	3.222	—	0.79
$S_1$	3.638	1.16	0.66	3.318	1.22	0.64	3.91	0.93	0.95
$\Delta E^{ST}$	<b>0.754</b>			<b>0.731</b>			<b>0.687</b>		

State	PTZ–OXD			PTZ–TDZ			PTZ–TAZ		
	$E$ (eV)	O.S.	$\phi_s$	$E$ (eV)	O.S.	$\phi_s$	$E$ (eV)	O.S.	$\phi_s$
$T_1$	2.883	—	0.82	2.592	—	0.80	3.214	—	0.83
$S_1$	3.660	1.22	0.68	3.361	1.30	0.67	3.892	0.91	0.64
$\Delta E^{ST}$	<b>0.777</b>			<b>0.769</b>			<b>0.678</b>		

State	2PXZ–OXD			2PXZ–TDZ			2PXZ–TAZ		
	$E$ (eV)	O.S.	$\phi_s$	$E$ (eV)	O.S.	$\phi_s$	$E$ (eV)	O.S.	$\phi_s$
$T_1$	2.810	—	0.81	2.522	—	0.79	3.148	—	0.82
$S_1$	3.515	1.75	0.72	3.226	1.84	0.69	3.786	1.44	0.82
$\Delta E^{ST}$	<b>0.705</b>			<b>0.704</b>			<b>0.638</b>		

State	2PTZ–OXD			2PTZ–TDZ			2PTZ–TAZ		
	$E$ (eV)	O.S.	$\phi_s$	$E$ (eV)	O.S.	$\phi_s$	$E$ (eV)	O.S.	$\phi_s$
$T_1$	2.821	—	0.82	2.511	—	0.80	3.138	—	0.82
$S_1$	3.549	1.74	0.74	3.227	1.41	0.71	3.759	1.95	0.90
$\Delta E^{ST}$	<b>0.728</b>			<b>0.716</b>			<b>0.622</b>		

<sup>a</sup> Note that the oscillator strengths are only defined for singlet excitations.

**Table 3** Relaxation energies ( $\lambda_{rel}$ ) and  $\Delta E^{ST}$  calculated for the first singlet ( $S_1$ ) and triplet ( $T_1$ ) excited states

	PXZ–OXD	PXZ–TDZ	PXZ–TAZ
$\lambda_{S_1}$ (eV)	0.27	0.25	0.33
$\lambda_{T_1}$ (eV)	0.27	0.24	0.37
$\Delta E^{ST}$	<b>0.009</b>	<b>0.007</b>	<b>0.11</b>

	PTZ–OXD	PTZ–TDZ	PTZ–TAZ
$\lambda_{S_1}$ (eV)	0.51	0.50	0.57
$\lambda_{T_1}$ (eV)	0.50	0.49	0.53
$\Delta E^{ST}$	<b>0.008</b>	<b>0.006</b>	<b>0.13</b>

	2PXZ–OXD	2PXZ–TDZ	2PXZ–TAZ
$\lambda_{S_1}$ (eV)	0.19	0.20	0.24
$\lambda_{T_1}$ (eV)	0.19	0.19	0.34
$\Delta E^{ST}$	<b>0.008</b>	<b>0.006</b>	<b>0.11</b>

	2PTZ–OXD	2PTZ–TDZ	2PTZ–TAZ
$\lambda_{S_1}$ (eV)	0.36	0.37	0.41
$\lambda_{T_1}$ (eV)	0.35	0.36	0.32
$\Delta E^{ST}$	<b>0.008</b>	<b>0.005</b>	<b>0.010</b>

is compatible with an increase in the rate of the energy transfer process. In addition, the delayed fluorescence spectrum matches perfectly the emission spectrum of the equatorial conformer highlighting the efficient up-conversion of triplet excitons into singlets (resulting in OLEDs with EQE of 10.8%) characteristic of an emitter exploiting a TADF mechanism.

Combining all these elements together, the coexistence of two conformers does not appear to be a key limitation in order for a compound to work as an efficient TADF emitter.

### 3.3 Conformation influence on the oscillator strength and singlet–triplet splitting

We have so far demonstrated that both D–A and D–A–D systems could act as efficient TADF materials exhibiting an extremely small singlet–triplet splitting gap. However, the oscillator strengths of these compounds vanish because of the pronounced CT character of their  $S_1$  state. Interestingly, TADF emitters exhibit usually quite broad emission spectra which in general are associated with the conformational disorder due to their high molecular flexibility.<sup>66</sup> When focusing on the equatorial conformers, the torsion energy profiles appear to be rather flat (see again Fig. 6) suggesting the possibility of thermally-activated variations in the D–A torsion angle, of up to 45 degrees around the minimum of the potential energy surface. As expected, the  $\Delta E_V^{ST}$  decreases when the D–A torsion angle is increased (see Fig. 7 top left panel for **PXZ–OXD** and top right panel for **PTZ–TAZ**, respectively) which comes along with an increase of the CT character of the  $S_1$  state in agreement with the decrease of  $\phi_s(S_1)$  (see Fig. 7 bottom left panel for **PXZ–OXD** and bottom right panel for **PTZ–TAZ**). Similarly, the CT character of the **PXZ–OXD**  $T_1$  state increases ( $\phi_s(T_1)$  decreases) when increasing the D–A torsion angle. Not surprisingly, for the equatorial conformer, the CT states are stabilized with respect to their corresponding LE states because of the twisted conformation. In great contrast to **PXZ–OXD**,  $\phi_s(T_1)$  for **PTZ–TAZ** is almost constant (having a LE character) irrespective of the value of the dihedral angle between the PTZ donor and the TAZ acceptor, consistent with its larger  $\Delta E_V^{ST}$  compared to other D–A compounds. In addition, the oscillator strength increases significantly when going out of the equatorial minimum of the potential energy surface, since the overlap between the hole and electron densities (*i.e.*  $\phi_s(S_1)$ ) increases. Actually, we have found that the oscillator strength exhibits a linear relation with  $[\phi_s(S_1)]^2$  and does not thus deviate from its definition (see Fig. S16, ESI†). Light emission is then likely to be assisted by soft vibrational modes in these series of compounds, which could appear as a general feature of efficient TADF emitters. In Table 4, we have calculated the Boltzmann-averaged  $\Delta E_V^{ST}$  and oscillator strengths for the PXZ- and PTZ-based D–A compounds and observed a significant increase of both quantities compared to the values obtained for the optimized geometries in Table 1. We also note that  $\Delta E_V^{ST}$  standard deviations are as large as the average values, implying that different conformations will contribute preferentially either to the light emission or to the up-conversion of triplet excitons into singlet ones. Experimental inspection of the PL properties of **2PXZ–OXD** and **2PXZ–TAZ** molecules in solution reveals that in view of the reported<sup>30</sup> PLQY values, D–A–D molecules (*i.e.* **2PXZ–OXD** and **2PXZ–TAZ**) can emit more total (prompt and delayed) fluorescence than the D–A ones. For D–A–D compounds, we have evaluated the torsion profiles of **2PXZ–OXD**, **2PXZ–TDZ** and **2PXZ–TAZ** by varying both D–A torsion angles ( $\phi_1$  and  $\phi_2$ ) between 0 and 90 degrees resulting in two dimensional maps (see Fig. S17, ESI†) which

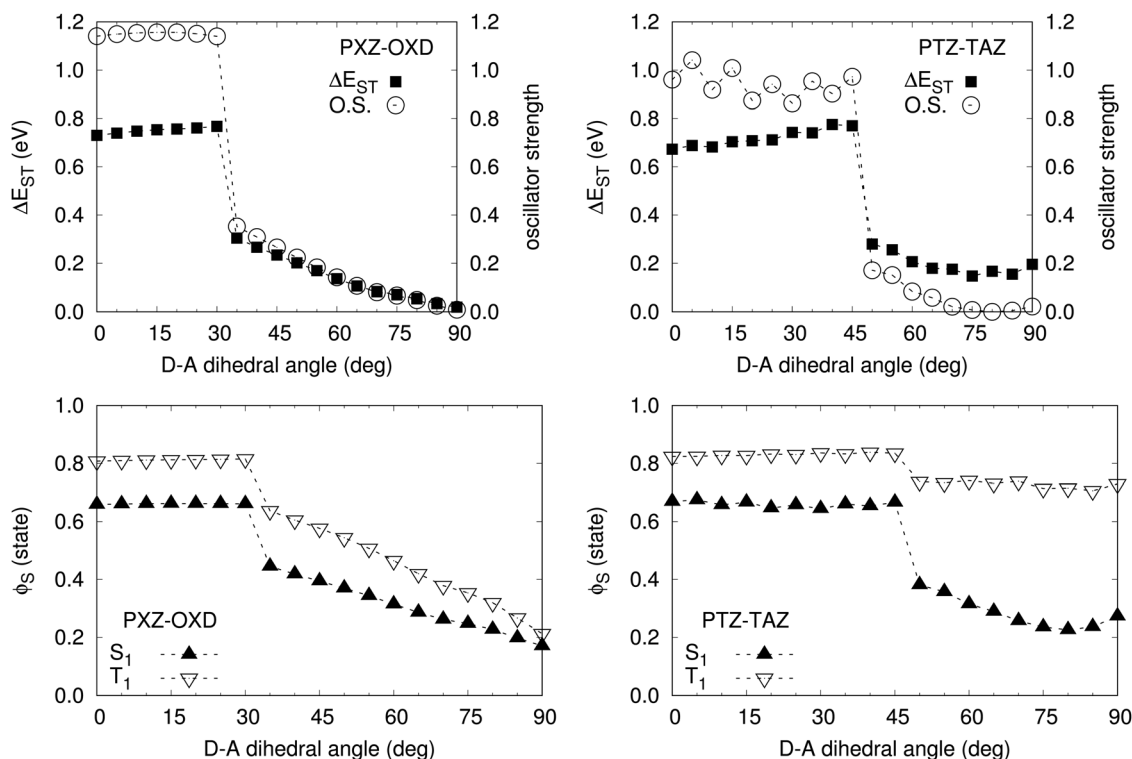


Fig. 7  $\Delta E^{\text{ST}}$  and oscillator strength (O.S.) (top panels) and  $\phi_{\text{S}}(\text{S}_1)$  and  $\phi_{\text{S}}(\text{T}_1)$  (bottom panels) obtained at the TDA-PBE0-D3(BJ)/6-31G(d,p) level of theory with the PCM module for solvent (toluene), calculated for **PXZ-OXD** (left panels) and **PTZ-TAZ** (right panels) as a function of the torsion angle between their respective donor and OXD acceptor units.

Table 4 Boltzmann-averaged  $\Delta E^{\text{ST}}$ , oscillator strengths and  $\phi_{\text{S}}$  for  $\text{S}_1$  and  $\text{T}_1$  of D-A compounds and 2PXZ derivatives

	PXZ-OXD	PXZ-TDZ	PXZ-TAZ
$\Delta E^{\text{ST}}$ (eV)	0.095 ± 0.102	0.076 ± 0.096	0.071 ± 0.065
O.S.	0.101 ± 0.152	0.094 ± 0.094	0.049 ± 0.046
$\phi_{\text{S}}(\text{T}_1)$	0.37 ± 0.11	0.32 ± 0.13	0.40 ± 0.13
$\phi_{\text{S}}(\text{S}_1)$	0.26 ± 0.08	0.26 ± 0.08	0.24 ± 0.07
	PTZ-OXD	PTZ-TDZ	PTZ-TAZ
$\Delta E^{\text{ST}}$ (eV)	0.055 ± 0.043	0.078 ± 0.054	0.183 ± 0.017
O.S.	0.025 ± 0.035	0.061 ± 0.061	0.022 ± 0.027
$\phi_{\text{S}}(\text{T}_1)$	0.41 ± 0.11	0.47 ± 0.07	0.73 ± 0.01
$\phi_{\text{S}}(\text{S}_1)$	0.21 ± 0.04	0.22 ± 0.05	0.26 ± 0.03
	2PXZ-OXD	2PXZ-TDZ	2PXZ-TAZ
$\Delta E^{\text{ST}}$ (eV)	0.061 ± 0.034	0.055 ± 0.036	0.057 ± 0.038
O.S.	0.081 ± 0.079	0.104 ± 0.101	0.049 ± 0.067
$\phi_{\text{S}}(\text{T}_1)$	0.39 ± 0.08	0.37 ± 0.09	0.40 ± 0.13
$\phi_{\text{S}}(\text{S}_1)$	0.23 ± 0.06	0.21 ± 0.06	0.21 ± 0.06

confirmed that the equatorial geometries are the most stable for all 2PXZ D-A-D compounds considered here. In addition,  $\Delta E^{\text{ST}}$  and oscillator strength are minimal at these geometries (see Fig. S18 and S19, ESI<sup>†</sup> respectively) in agreement with an increase of the CT character with respect to the D-A compounds (see  $\phi_{\text{S}}(\text{S}_1)$  and  $\phi_{\text{S}}(\text{T}_1)$  maps in Fig. S20 and S21, ESI<sup>†</sup> respectively).

Overall, moving away from the global (equatorial) minimum, we note an increase  $\Delta E^{\text{ST}}$  for both D-A and D-A-D systems, followed by an increase in average  $\phi_{\text{S}}(\text{T}_1)$  compared to a more

modest for  $\phi_{\text{S}}(\text{S}_1)$  which confers to  $\text{T}_1$  a mixed CT-LE character, while  $\text{S}_1$  remains a CT-like state and is much less affected by the torsional dynamics. The Boltzmann-averaged oscillator strength for the 2PXZ molecules is comparable to the oscillator strength calculated for PXZ compounds. This feature comes along with lower average  $\Delta E^{\text{ST}}$  for 2PXZ derivatives, as well as lower standard deviations with respect to PXZ molecules. It appears to be linked to the relative insensitivity of both  $\Delta E^{\text{ST}}$  and the oscillator strength to the variation in torsion angle ( $\phi_1$  and  $\phi_2$ ) beyond 60 degrees (see Fig. S18 and S19, ESI<sup>†</sup>). The lower  $\Delta E^{\text{ST}}$  standard deviations and the similar averaged oscillator strengths for 2PXZ molecules with respect to D-A systems suggest that, for the D-A-D compounds, a set of conformers with rather low  $\Delta E^{\text{ST}}$  contributes both to the triplet-singlet interconversion and to light emission. These factors prompt us to hypothesize that in real devices D-A-D compounds could behave more efficiently than D-A ones.

## 4 Conclusions

We have carried out an in-depth theoretical study to characterize, and further engineer, a set of new TADF emitters based on combining adequate donor (PXZ, PTZ) and acceptor (OXD, TDZ, TAZ) chromophores following the D-A or D-A-D sequence. Since good candidates for TADF should possess spatially separated frontier orbitals, a feature directly related to a low singlet-triplet energy gap, we have explored this issue by relying on the attachment/detachment formalism simplifying the description of the excitations. Based on this formalism, we have calculated

the electron–hole separation  $\Delta r$  and the overlap between the hole and electron densities  $\phi_s$  associated with the excitation. Among the two indexes,  $\phi_s$  appears to be the most reliable one for assigning the correct nature (CT or LE) of the lowest excited states for both non-symmetric D–A and symmetric D–A–D compounds. We have also found that for PXZ-based compounds, equatorial conformers are more stable than axial ones while for PTZ-based compounds, there is most likely a coexistence of equatorial and axial conformers because of the small energy difference between these conformers. Still, for both donors, the equatorial conformers are expected to contribute predominantly to the RISC process since their singlet–triplet gap is much smaller. Indeed, their low  $\Delta E^{\text{ST}}$  values are associated with lowest singlet and triplet transitions exhibiting a strong CT character and thus  $\phi_s$  values close to 0.

We have also identified that connecting donor and acceptor units in a twisted conformation (*i.e.* equatorial conformation) is a necessary condition but not sufficient for obtaining the spatial separation between the hole and electron densities associated with low  $\Delta E^{\text{ST}}$  values. In terms of the light-emitting properties, we have demonstrated that oscillator strengths for the series of compounds studied here vanish in the equatorial conformations at their optimized ground and first singlet excited state geometries. However, the torsional potential of all these compounds is flat enough to make them able, even at room temperature, to access a set of conformations displaying non-negligible oscillator strengths, hence light emission appears to be a vibrationally assisted process in these compounds. In addition, we have rationalized the experimental observation that D–A–D compounds emit more light than D–A ones, since: (a)  $\Delta E^{\text{ST}}$  average (over the different configurations considered) and the corresponding standard deviations are smaller for D–A–D molecules, and (b) averaged oscillator strengths are still comparable. The overall superior TADF properties of D–A–D systems appear to be a consequence of the largest number of donor units connected to the central acceptor with a considerable number of D–A–D conformations to participate in the interconversion between triplet and singlet excitons as well as the light emission, which is not the case for D–A compounds.

## Acknowledgements

This work was partially supported by the Samsung Advanced Institute of Technology (SAIT)'s Global Research Outreach (GRO) Program. In addition, the research in Bordeaux has been funded by the French State grant ANR-10-LABX-0042-AMADEus managed by the French National Research Agency under the initiative of excellence IdEx Bordeaux program (reference ANR-10-IDEX-0003-02). The work in Mons was supported by the “Programme d'Excellence de la Région Wallonne” (OPTI2MAT project) and FNRS-FRFC. Computational resources have been provided by the Consortium des Équipements de Calcul Intensif (CÉCI), funded by the Fonds de la Recherche Scientifique de Belgique (F.R.S.-FNRS) under Grant no. 2.5020.11 as well as the Tier-1 supercomputer of the Fédération Wallonie-Bruxelles,

infrastructure funded by the Walloon Region under the grant agreement no. 1117545. Mónica Moral thanks to the E2TP CYTEMA-Santander Program for their financial support. We acknowledge stimulating discussions with Prof. Antonio Monari and Dr Thibaut Etienne from the University of Lorraine on the attachment/detachment formalism as well as on the use of the NANCY\_EX package. The authors are grateful to Dr Vincent Lemaur for critical reading of the manuscript.

## References

- 1 K. Müllen and U. Scherf, *Organic Light-Emitting Devices*, 2006.
- 2 A. Endo, K. Sato, K. Yoshimura, T. Kai, A. Kawada, H. Miyazaki and C. Adachi, *Appl. Phys. Lett.*, 2011, **98**, 083302.
- 3 T. Nakagawa, S.-Y. Ku, K.-T. Wong and C. Adachi, *Chem. Commun.*, 2012, **48**, 9580–9582.
- 4 Q. Zhang, J. Li, K. Shizu, S. Huang, S. Hirata, H. Miyazaki and C. Adachi, *J. Am. Chem. Soc.*, 2012, **134**, 14706–14709.
- 5 H. Uoyama, K. Goushi, K. Shizu, H. Nomura and C. Adachi, *Nature*, 2012, **492**, 234–238.
- 6 K. Sato, K. Shizu, K. Yoshimura, A. Kawada, H. Miyazaki and C. Adachi, *Phys. Rev. Lett.*, 2013, **110**, 247401.
- 7 H. Yersin, A. Rausch, R. Czerwieniec, T. Hofbeck and T. Fischer, *Coord. Chem. Rev.*, 2011, **255**, 2622–2652.
- 8 C. Brown and D. Kondakov, *J. Soc. Inf. Disp.*, 2004, **12**, 323–327.
- 9 A. Endo, M. Ogasawara, A. Takahashi, D. Yokoyama, Y. Kato and C. Adachi, *Adv. Mater.*, 2009, **21**, 4802–4806.
- 10 K. Goushi, K. Yoshida, K. Sato and C. Adachi, *Nat. Photonics*, 2012, **6**, 253–258.
- 11 T. Serevičius, T. Nakagawa, M.-C. Kuo, S.-H. Cheng, K.-T. Wong, C.-H. Chang, R. Kwong, S. Xia and C. Adachi, *Phys. Chem. Chem. Phys.*, 2013, **15**, 15850–15855.
- 12 K. Udagawa, H. Sasabe, C. Cai and J. Kido, *Adv. Mater.*, 2014, **26**, 5062–5066.
- 13 Q. Wang, I. Oswald, X. Yang, G. Zhou, H. Jia, Q. Qiao, Y. Chen, J. Hoshikawa-Halbert and B. Gnade, *Adv. Mater.*, 2014, **26**, 8107–8113.
- 14 Y. Tao, K. Yuan, T. Chen, P. Xu, H. Li, R. Chen, C. Zheng, L. Zhang and W. Huang, *Adv. Mater.*, 2014, **26**, 7931–7958.
- 15 K. Shizu, H. Tanaka, M. Uejima, T. Sato, K. Tanaka, H. Kaji and C. Adachi, *J. Phys. Chem. C*, 2015, **119**, 1291–1297.
- 16 Q. Zhang, B. Li, S. Huang, H. Nomura, H. Tanaka and C. Adachi, *Nat. Photonics*, 2014, **8**, 326–332.
- 17 R. Nobuyasu, Z. Ren, G. Griffiths, A. Batsanov, P. Data, S. Yan, A. Monkman, M. Bryce and F. Dias, *Adv. Opt. Mater.*, 2016, **4**, 648–653.
- 18 P. L. Santos, J. S. Ward, P. Data, A. S. Batsanov, M. R. Bryce, F. B. Dias and A. P. Monkman, *J. Mater. Chem. C*, 2016, **4**, 3815–3824.
- 19 J. Gibson, A. P. Monkman and T. J. Penfold, *ChemPhysChem*, 2016, **17**, 2956–2961.
- 20 T. Ogiwara, Y. Wakikawa and T. Ikoma, *J. Phys. Chem. A*, 2015, **119**, 3415–3418.

- 21 S. Huang, Q. Zhang, Y. Shiota, T. Nakagawa, K. Kuwabara, K. Yoshizawa and C. Adachi, *J. Chem. Theory Comput.*, 2013, **9**, 3872–3877.
- 22 T. Penfold, *J. Phys. Chem. C*, 2015, **119**, 13535–13544.
- 23 H. Sun, C. Zhong and J.-L. Brédas, *J. Chem. Theory Comput.*, 2015, **11**, 3851–3858.
- 24 Y. Shu and B. Levine, *J. Chem. Phys.*, 2015, **142**, 104104.
- 25 R. Gomez-Bombarelli, J. Aguilera-Iparraguirre, T. D. Hirzel, D. Duvenaud, D. Maclaurin, M. A. Blood-Forsythe, H. S. Chae, M. Einzinger, D.-G. Ha, T. Wu, G. Markopoulos, S. Jeon, H. Kang, H. Miyazaki, M. Numata, S. Kim, W. Huang, S. I. Hong, M. Baldo, R. P. Adams and A. Aspuru-Guzik, *Nat. Mater.*, 2016, **15**, 1120–1127.
- 26 B. Milián-Medina and J. Gierschner, *Org. Electron.*, 2012, **13**, 985–991.
- 27 S. Hirata, Y. Sakai, K. Masui, H. Tanaka, S. Lee, H. Nomura, N. Nakamura, M. Yasumatsu, H. Nakanotani, Q. Zhang, K. Shizu, H. Miyazaki and C. Adachi, *Nat. Mater.*, 2015, **14**, 330–336.
- 28 M. Kim, S. Jeon, S.-H. Hwang and J. Lee, *Adv. Mater.*, 2015, **27**, 2515–2520.
- 29 H. Tanaka, K. Shizu, H. Nakanotani and C. Adachi, *Chem. Mater.*, 2013, **25**, 3766–3771.
- 30 J. Lee, K. Shizu, H. Tanaka, H. Nomura, T. Yasuda and C. Adachi, *J. Mater. Chem. C*, 2013, **1**, 4599–4604.
- 31 H. Tanaka, K. Shizu, J. Lee and C. Adachi, *J. Phys. Chem. C*, 2015, **119**, 2948–2955.
- 32 M. Moral, L. Muccioli, W.-J. Son, Y. Olivier and J. Sancho-Garca, *J. Chem. Theory Comput.*, 2015, **11**, 168–177.
- 33 H. Tian, X. Yang, R. Chen, Y. Pan, L. Li, A. Hagfeldt and L. Sun, *Chem. Commun.*, 2007, 3741–3743.
- 34 S. Agrawal, M. Pastore, G. Marotta, M. A. Reddy, M. Chandrasekharam and F. D. Angelis, *J. Phys. Chem. C*, 2013, **117**, 9613–9622.
- 35 W. Zhou, Y. Wen, L. Ma, Y. Liu and X. Zhan, *Macromolecules*, 2012, **45**, 4115–4121.
- 36 B. Kim, J. Lee, Y. Park, C. Lee and J. Park, *J. Nanosci. Nanotechnol.*, 2014, **14**, 6404–6408.
- 37 S. Elkassih, P. Sista, H. Magurudeniya, A. Papadimitratos, A. Zakhidov, M. Biewer and M. Stefan, *Macromol. Chem. Phys.*, 2013, **214**, 572–577.
- 38 K. Kamtekar, K. Dahms, A. Batsanov, V. Jankus, H. Vaughan, A. Monkman and M. Bryce, *J. Polym. Sci., Part A: Polym. Chem.*, 2011, **49**, 1129–1137.
- 39 H. Tanaka, K. Shizu, H. Nakanotani and C. Adachi, *J. Phys. Chem. C*, 2014, **118**, 15985–15994.
- 40 J. Perdew, M. Ernzerhof and K. Burke, *J. Chem. Phys.*, 1996, **105**, 9982–9985.
- 41 C. Adamo and V. Barone, *J. Chem. Phys.*, 1999, **110**, 6158–6170.
- 42 A. Becke and E. Johnson, *J. Chem. Phys.*, 2005, **123**, 154101.
- 43 S. Grimme, J. Antony, S. Ehrlich and H. Krieg, *J. Chem. Phys.*, 2010, **132**, 154104.
- 44 S. Grimme, S. Ehrlich and L. Goerigk, *J. Comput. Chem.*, 2011, **32**, 1456–1465.
- 45 S. Hirata and M. Head-Gordon, *Chem. Phys. Lett.*, 1999, **314**, 291–299.
- 46 M. Peach, M. Williamson and D. Tozer, *J. Chem. Theory Comput.*, 2011, **7**, 3578–3585.
- 47 M. Peach and D. Tozer, *J. Phys. Chem. A*, 2012, **116**, 9783–9789.
- 48 M. Peach, N. Warner and D. Tozer, *Mol. Phys.*, 2013, **111**, 1271–1274.
- 49 J. Tomasi, B. Mennucci and R. Cammi, *Chem. Rev.*, 2005, **105**, 2999–3093.
- 50 G. Scalmani and M. Frisch, *J. Chem. Phys.*, 2010, **132**, 114110.
- 51 M. J. Frisch, G. W. Trucks, H. B. Schlegel, G. E. Scuseria, M. A. Robb, J. R. Cheeseman, G. Scalmani, V. Barone, B. Mennucci, G. A. Petersson, H. Nakatsuji, M. Caricato, X. Li, H. P. Hratchian, A. F. Izmaylov, J. Bloino, G. Zheng, J. L. Sonnenberg, M. Hada, M. Ehara, K. Toyota, R. Fukuda, J. Hasegawa, M. Ishida, T. Nakajima, Y. Honda, O. Kitao, H. Nakai, T. Vreven, J. A. Montgomery, Jr., J. E. Peralta, F. Ogliaro, M. Bearpark, J. J. Heyd, E. Brothers, K. N. Kudin, V. N. Staroverov, R. Kobayashi, J. Normand, K. Raghavachari, A. Rendell, J. C. Burant, S. S. Iyengar, J. Tomasi, M. Cossi, N. Rega, J. M. Millam, M. Klene, J. E. Knox, J. B. Cross, V. Bakken, C. Adamo, J. Jaramillo, R. Gomperts, R. E. Stratmann, O. Yazyev, A. J. Austin, R. Cammi, C. Pomelli, J. W. Ochterski, R. L. Martin, K. Morokuma, V. G. Zakrzewski, G. A. Voth, P. Salvador, J. J. Dannenberg, S. Dapprich, A. D. Daniels, O. Farkas, J. B. Foresman, J. V. Ortiz, J. Cioslowski and D. J. Fox, *Gaussian09 Revision A.01*, Gaussian Inc., Wallingford CT, 2009.
- 52 F. Weigend and R. Ahlrichs, *Phys. Chem. Chem. Phys.*, 2005, **7**, 3297–3305.
- 53 T. Chen, L. Zheng, J. Yuan, Z. An, R. Chen, Y. Tao, H. Li, X. Xie and W. Huang, *Sci. Rep.*, 2015, **5**, 10923.
- 54 M. Peach, P. Benfield, T. Helgaker and D. Tozer, *J. Chem. Phys.*, 2008, **128**, 044118.
- 55 M. Head-Gordon, A. M. Grana, D. Maurice and C. A. White, *J. Phys. Chem.*, 1995, **99**, 14261–14270.
- 56 A. Dreuw and M. Head-Gordon, *Chem. Rev.*, 2005, **105**, 4009–4037.
- 57 C. Guido, P. Cortona, B. Mennucci and C. Adamo, *J. Chem. Theory Comput.*, 2013, **9**, 3118–3126.
- 58 T. Etienne, X. Assfeld and A. Monari, *J. Chem. Theory Comput.*, 2014, **10**, 3896–3905.
- 59 T. Etienne, X. Assfeld and A. Monari, *J. Chem. Theory Comput.*, 2014, **10**, 3906–3914.
- 60 M. Grüning, A. Marini and X. Gonze, *Nano Lett.*, 2009, **9**, 2820–2824.
- 61 Z. Grabowski, K. Rotkiewicz and W. Rettig, *Chem. Rev.*, 2003, **103**, 3899–4031.
- 62 A. Köhler and D. Beljonne, *Adv. Funct. Mater.*, 2004, **14**, 11–18.
- 63 A. Köhler and H. Bässler, *Mater. Sci. Eng., R*, 2009, **66**, 71–109.
- 64 D. Jacquemin, E. Perpète, I. Ciofini and C. Adamo, *J. Comput. Chem.*, 2008, **29**, 921–925.
- 65 J. Sears, T. Koerzdoerfer, C.-R. Zhang and J.-L. Brédas, *J. Chem. Phys.*, 2011, **135**, 151103.
- 66 M. Moral, W.-J. Son, J. Sancho-Garca, Y. Olivier and L. Muccioli, *J. Chem. Theory Comput.*, 2015, **11**, 3383–3392.